analytical chemistry

Article

pubs.acs.org/ac

Real Time Monitoring of Layer-by-Layer Polyelectrolyte Deposition and Bacterial Enzyme Detection in Nanoporous Anodized Aluminum Oxide

Fransiska Sri Herwahyu Krismastuti,[†,‡] Haider Bayat,[§] Nicolas H. Voelcker,*[,†,‡] and Holger Schönherr*[,§]

[†]ARC Centre of Excellence in Convergent Bio-Nano Science and Technology, Mawson Institute, University of South Australia, Mawson Lakes, Adelaide, South Australia 5095, Australia

[‡]Wound Management Innovation Cooperative Research Centre, University of South Australia, Mawson Lakes, Adelaide, South Australia 5095, Australia

[§]Physical Chemistry I, Department of Chemistry and Biology, University of SiegenAdolf-Reichwein-Str. 2, 57076 Siegen, Germany

Supporting Information

ABSTRACT: Porous anodized aluminum oxide (pAAO) is a nanostructured material, which due to its optical properties lends itself to the design of optical biosensors where interactions in the pores of this material are transduced into interferometric reflectance shifts. In this study, a pAAO-based biosensor was developed as a biosensing platform to detect proteinase K, an enzyme which is a readily available model system for the proteinase produced by *Pseudomonas aeruginosa*. The pAAO pore walls are decorated by means of the layer-by-layer (LbL) deposition technique using poly(sodium-4-styrenesulfonate) and poly-L-lysine as negatively and positively charged polyelectrolytes, respectively. Interferometric reflectance spectroscopy utilized to observe the optical properties of pAAO during LbL deposition shows that the deposition of the polyelectrolyte onto the pore walls increases the net refractive index, thus red-shifting the effective optical thickness (EOT). Upon incubation with proteinase K, a conspicuous blue shift of the EOT is observed, which is attributed to the destabilization of the LbL film upon enzymatic degradation of the poly-L-lysine components. This result is confirmed by scanning electron microscopy results. Finally, as a proof-of-principle, we demonstrate the ability of the label-free pAAO-based biosensing platform to detect the presence of the proteinase K in human wound fluid, highlighting the potential for detection of bacterial infections in chronic wounds.

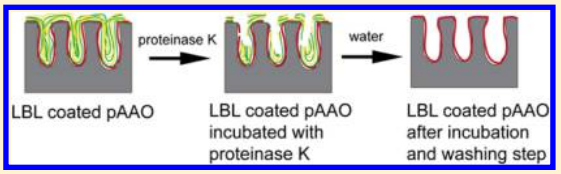

Porous anodized aluminum oxide (pAAO) is a material featuring close-packed hexagonal arrays of cylindrical nanoscale pores. pAAO has unique optical properties that predispose this material for sensing applications, exploiting, e.g., changes in photoluminescence, transmittance, reflectivity, absorbance, impedance, and conductance.[1−4] In addition, due to its physical and chemical attributes, such as large surface area, high stability in biological medium, and ease of surface functionalization, this material is becoming a promising alternative to other popular sensor materials such as porous silicon (pSi).[1,5−10]

A common transducer mechanism for pAAO and pSi is interferometric reflectance spectroscopy (IRS).[1] White light illumination of a thin film of pAAO on Al generates a Fabry-Pérot fringe pattern, and this pattern allows the extraction of the physical characteristics of the film, such as refractive index and film thickness. Peak and valley positions in the pattern are determined by the relationship $m\lambda = 2nd$, where λ is the wavelength of the maximum of the consecutive interference of order m and n is refractive index of the film with a thickness d. The term "$2nd$" is called the effective optical thickness (EOT) and is directly obtained from the fringe pattern by fast Fourier transformation. Thus, analyte detection is in practice achieved by monitoring changes in the EOT over time, as molecules bind to or are removed from the pAAO film.[11−13] To improve the fidelity of the fringe pattern obtained from pAAO, we recently reported that an ultrathin semi-reflective noble metal coating improves the fidelity of the fringe pattern obtained from pAAO.[1]

Surface functionalization of the pAAO is a prerequisite for biorecognition in the pAAO film. The common surface functionalization chemistries for pAAO include silanization,[14,15] polymer grafting,[16] sol−gel modification,[17] layer-by-layer (LbL) deposition,[18−20] and electroless deposition.[21] Here, instead of immobilizing a receptor for the analyte on the pAAO walls to bind the analyte, we decided to coat the pore walls via LbL with polyelectrolyte layers that are degraded by the target enzyme analyte.

Bacterial infections in wounds lead to bacterial colonization and biofilm formation.[22,23] Sometimes, early detection of wound infections is difficult since the clinical symptoms are not clear.[24] Certain bacterial infections contribute to a poor healing status of chronic wounds and are responsible for the mortality of chronic wound patients due to sepsis.[23,25] To make

Received: December 12, 2014
Accepted: March 4, 2015

ACS Publications © XXXX American Chemical Society

DOI: 10.1021/ac504626m
Anal. Chem. XXXX, XXX, XXX−XXX

matters worse, established biofilms are rather resistant to antibiotic treatments.[23,25] Among the wound colonizing bacterial species, *Pseudomonas aeruginosa* is the most common Gram-negative pathogenic bacteria found in biofilms of nonhealing wounds.[23,26] Therefore, an important strategy in chronic wounds treatment is the early detection of this biofilm forming bacteria.

The standard procedures for bacterial diagnostics are swab cultures or tissue biopsies,[24,27] which are time-consuming and costly. As an alternative to detect bacterial infection, Tücking et al.[28] developed a different approach targeting specific enzyme secreted by the bacteria. In their study, they use biodegradable enzyme-responsive polymersomes to detect proteinase K, which is a readily available model enzyme for the proteinase produced by *Pseudomonas aeruginosa*.[29] Proteinase K is able to degrade poly(ethylene glycol)-*block*-poly(lactic acid) (PEG-*b*-PLA) polymersomes, which contain a fluorescent dye that is released upon degradation. This straightforward approach, which has been validated with a bacterial supernatant of *Pseudomonas aeruginosa* containing proteinases, can also fulfill a therapeutic function, whereby an antimicrobial is released.

In this study, we develop a pAAO-based optical diagnostic tool for proteinase K detection as a *Pseudomonas aeruginosa* surrogate. The pAAO is utilized as porous matrix to immobilize the biorecognition molecules by means of the LbL approach. The deposition of LbL and detection of the enzyme is monitored by means of IRS since the layer formation and degradation induce changes in refractive index of the pAAO structure. A similar approach, but in the pSi structure, was employed by Kilian et al.[30] and Orosco et al.[31] They coated the pSi rugate filter using protease sensitive polymer (gelatin)[30] or protein[31] as biorecognition molecules. Digestion of the sensitive polymer or protein changes the refractive index of pSi film shifting the position of the photonic peak.

In our study, the LbL multilayer of anionic and cationic polyelectrolytes is built up in the nanoporous AAO structure. The polyelectrolytes consist of poly(sodium-4-styrenesulfonate) (PSS) and poly-L-lysine (PLL) as an anionic and a cathionic polyelectrolyte, respectively. The peptide bonds in PLL are cleavable by proteinase K, and this destabilizes the LbL film. Loss of LbL coating decreases the refractive index of the porous layer, leading to the blue shift of the EOT. Once we studied the performance of this biosensor, we demonstrated bacterial enzyme detection using wound fluid samples taken from chronic wound patients.

MATERIALS AND METHODS

Fabrication and Characterization of the pAAO. The pAAO was fabricated from an ultra high purity (99.9999%, 0.5 mm thick plate, Chempure) aluminum using a two-step mild anodization process[32] in a Teflon cell. Prior to anodization, the aluminum surface was washed using acetone, dried under a stream of nitrogen gas, and immersed in 0.5 M sodium hydroxide (C.N. 1310-73-2, Sigma-Aldrich). After a 10 min immersion, the aluminum was rinsed with Milli-Q water (from a Millipore Direct-Q 8 System with resistivity of 18.0 MΩcm, Millipore, Schwalbach, Germany) and dried under a stream of nitrogen gas.

The precleaned aluminum was electropolished using electropolishing solution containing 4.2 M perchloric acid (60−62%, J.T. Baker) in ethanol. The electropolishing was conducted at room temperature for 3 min at a constant voltage of 20 V and a current of 0.14 A. After electropolishing, the aluminum was removed from the cell, washed with Milli-Q water, and dried under a stream of nitrogen gas.

The electropolished samples were loaded in the anodization cell and anodized using a two-step anodization process. The first anodization was done for 14 h in 0.3 M oxalic acid (C.N. 6153-56-6, Merck) solution, at a constant voltage of 40 V and a current of 2 mA with the cell placed in a water bath at a constant temperature of 5 °C. The pAAO was then rinsed with Milli-Q water and dried under a stream of nitrogen gas. The formed porous layer was then removed in an aqueous solution containing 0.7 M phosphoric acid (85%, Chemische Fabrik Budenheim) and 0.2 M chromium oxide (C.N. 27081-50G-F, Sigma-Aldrich) for 5 h at 65 °C. Finally, the second anodization was conducted using the same procedure as for the first anodization, but for a shorter time (10, 20, or 30 min), depending on the desired thickness. The topography of the pAAO film was characterized using scanning electron microscopy (FE-SEM, Zeiss Ultra 55, Germany) with an accelerating voltage of 5 kV.

Interferometry Reflectance Spectroscopy (IRS). The reflectance spectra of the pAAO samples were obtained from an Ocean Optics spectrometer and a charge couple device (CCD) detector (USB 2000+) equipped with a tungsten halogen light source (LS-1). The data were collected using a SpectraSuite program, and the EOT was obtained by performing a fast Fourier transformation of the recorded interferometric reflectance spectra using Igor program (Wavemetrics Inc. Igor program).

LbL Deposition. The pAAO samples were functionalized by means of the LbL deposition technique. Before deposition, the pAAO sample was sonicated in water and dried under vacuum to clean the pores from any chemical residues. The pAAO sample was then silanized using neat (3-aminopropyl)-triethoxysilane (APTES, C.N. 919-30-2, 99%, Sigma-Aldrich) under vacuum for 15 h. The APTES functionalized pAAO surface was then sputter coated with gold for 1 min producing about a 7−10 nm gold layer. This metal layer has the additional advantage of preventing the pore blocking for this LbL film.[33]

LbL films were deposited into pAAO in a custom-made flow cell under IRS monitoring. The PSS (C.N. 25704-18-1, Sigma-Aldrich) and PLL (C.N. 25988-63-0, 0.1% w/v in H_2O, Sigma-Aldrich) solutions were prepared with the same concentration of 0.5 g/L in 0.15 M NaCl (C.N. 7647-14-5, Baker). The polyelectrolyte solution, PSS followed by PLL, was pumped into the flow cell at a flow rate of 0.2 mL/min. Rinsing steps using Milli-Q water were applied in between the incubations with oppositely charged polyelectrolytes.

Degradation of LbL Layers by Proteinase K. After the multilayer polyelectrolyte was deposited in the pores, the pAAO samples were then used to detect proteinase K from *Tritirachium album* (Sigma-Aldrich). The experiments were conducted in a custom-made flow cell under IRS monitoring. In the first 10 min, Milli-Q water was introduced to the samples, followed by exposure to proteinase K diluted in 20 mM phosphate buffer at pH 8 for 30 min, and then, a final rinse with Milli-Q water was applied.

Chronic Wound Fluid Experiment. The proteinase K detection was also conducted in a wound fluid sample. The wound fluid was gifted from Queen Elizabeth Hospital (South Australia, Australia). It was collected from patients with a chronic venous leg ulcer. The collection protocol conformed to the ethical guidelines of the 1975 Declaration of Helsinki and was approved by the Health Service Human Research Ethics

DOI: 10.1021/ac504626m
Anal. Chem. XXXX, XXX, XXX−XXX

Committee and Central Northern Adelaide Health Service Ethics of Human Research Committee. During sensing, Milli-Q water was first introduced to pAAO for 10 min, followed by a 10-fold dilution of wound fluid spiked with 0.5 mg/mL proteinase K for 30 min and a final wash with Milli-Q water.

RESULTS AND DISCUSSION

Fabrication and Characterization of pAAO Films. In this study, highly ordered pAAO was fabricated using a two-step electrochemical anodization process[34,35] and characterized by SEM (Figure S1a–c, Supporting Information). The anodization condition employed here produced pore diameters of 30 ± 1.7 nm, interpore distances of 100 ± 1.5 nm, and wall thicknesses of 70 ± 1.8 nm. The calculated porosity and pore density were 8% and 1.1×10^{11} pores/cm^2, respectively. Three different pAAO film thicknesses were fabricated using anodization times of 10, 20, and 30 min with the growth rate of 8.5 ± 0.6 μm/h, forming 1.3, 3.0, and 4.4 μm thick films, respectively (Figure S1d–f, Supporting Information).

LbL Deposition in pAAO. The ordered pAAO film was modified using the LbL approach by building up a PSS–PLL polyelectrolyte multilayer inside of the pores. PLL and PSS were dissolved in aqueous NaCl solutions in order to promote the polyelectrolyte adsorption onto the pore walls since the salt concentration determines the ionic strength of the solution and the thickness of the multilayer.[36−39] Increasing the salt concentration increases the ionic strength of the polyelectrolyte solution, hence increasing the thickness of multilayer. However, according the study conducted by Seyrek et al.,[40] this effect works until a salt concentration of 0.1 M and then plateau is observed. Thus, increasing the salt concentration above 0.1 M will not increase the thickness of the polyelectrolyte multilayer further. The experiments were carried out for a NaCl concentration of 0.15 M, which was found to be an optimum condition according to previous studies from our group[33] and also in agreement with the published study by Seyrek et al.[40]

The charge density of polyelectrolyte was found to be another important parameter to facilitate multilayer formation because this determines the conformation and the way polyelectrolyte adsorbed on the surface. In order to optimize adsorption, the polyelectrolyte should be sufficiently charged and this can be tuned by adjusting the pH of the polyelectrolyte solution. This pH effect is less relevant for strong polyelectrolyte such as PSS.[33,36,41] PLL however is a weak polyelectrolyte with a pK_a of 9, and lower pH solutions are required to promote and ionize this polymer, thus facilitating its adsorption on an oppositely charged surface. In this study, the pH for both the PSS and PLL was about 6, as the natural pH after preparation of the solution. In a similar study, pH 6 was determined as the optimum pH for the weak polyelectrolyte PAH (pK_a similar to PLL) in order to form a thick multilayer, as measured by ellipsometry.[33]

Figure 1a presents the schematic of the LbL deposition process in the porous layer of AAO. Before building up the multilayer polyelectrolyte, the pAAO was silanized using APTES to produce a positively charged surface that would subsequently be exposed to negatively charged PSS followed by positively charged PLL with Milli-Q water rinsing steps applied in between to remove any loosely bound unreacted molecules. The LbL deposition could be monitored in real time by IRS since the introduction of polyelectrolyte in the porous layer red-shifted the EOT. However, in order to do so, a thin layer of gold coating was required to increase the reflectivity of the pAAO film.[1] In addition, the gold film effectively suppresses the adsorption of an excess of polyelectrolyte near the pore mouth and affords almost filled pores.[33]

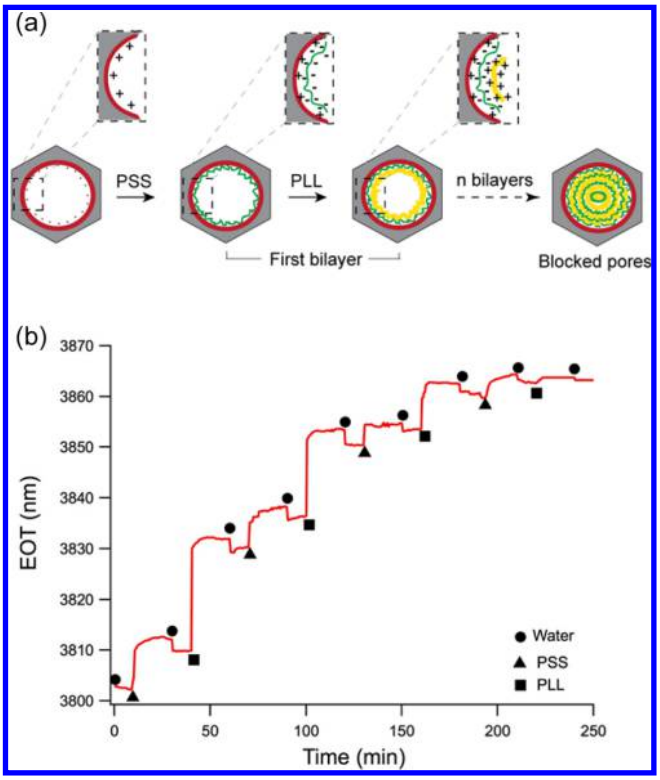

Figure 1. (a) Schematic of LbL deposition using PSS (green) and PLL (yellow) in a pAAO pore. The red trace indicates the APTES layer deposited before LbL. One LbL cycle consists of the deposition of one layer of PSS and one layer of PLL with rinsing steps in between. The cycle was repeated until the pores were blocked as indicated by a plateau EOT in IRS. (b) A typical IRS sensorgram during the LbL deposition process. This sensorgram was recorded for a pAAO sample anodized at 40 V for 10 min producing a 1.3 μm layer thickness. The black circles, black triangles, and black rectangles indicate the starting point of the exposure of the pAAO to Milli-Q water, PSS, and PLL, respectively.

Alternating LbL depositions of PSS and PLL into the pAAO film were carried out until the pores were completely blocked as indicated by an EOT plateau (Figure 1b) and confirmed by SEM (Figure S2, Supporting Information). A typical sensorgram acquired during LbL formation is presented in Figure 1b. From this figure, it can be seen that, in the first 10 min, when Milli-Q water was introduced to the surface, the EOT was constant. Upon the next exposure of the pAAO to pSS solution (11–30 min), the EOT increased by about 11 nm, confirming that the PSS had adsorbed to the amine-functional pAAO surface. The PSS solution was then further exposed to the pAAO until the EOT was constant (about 15 min exposure), which indicated that at this point a complete PSS layer had formed.

Washing with Milli-Q water (30–40 min) led to a small (2.2 nm) decrease in the EOT since unbound polyelectrolyte was removed as expected from previous studies using ellipsometry,[33] optical waveguide spectroscopy,[19] or small-angle X-ray scattering.[42] When the PLL solution was introduced into the cell comprising the pAAO surface for 20 min, a 25 nm increase in EOT indicated PLL binding. Once the EOT was constant,

DOI: 10.1021/ac504626m
Anal. Chem. XXXX, XXX, XXX–XXX

another Milli-Q washing step was applied, completing a full LbL cycle.

The LbL cycles were repeated until no further EOT increase was observed upon incubation with the oppositely charged polyelectrolyte. This plateau corresponded to either complete pore filling or pore blockage. For pAAO with a thickness of 1.3 μm, this effect was observed after deposition of four bilayers (Figure 1b). SEM imaging (Figure S2, Supporting Information) confirmed that the pores after two LbL cycles showed a reduced diameter and were completely closed after four cycles. Admittedly, it is difficult to distinguish between a blockage and complete pore filling from this top view.

The thickness changes on the interior pore surfaces due to multilayer formation were estimated using the Maxwell-Garnett equation[19,20] instead of the Bruggeman effective medium approximation. In the case of LbL inside the pores of pAAO, the Maxwell-Garnett theory has been used to determine the changes in dielectric function of separated phases of the composites contributed by the alumina, polyelectrolyte solutions, and polyelectrolyte layer coating the pore surfaces.[19,43] The dielectric function can be converted into the effective refractive index of the entire porous matrix that can be substituted to the Lorentz–Lorenz equation[43,44] to calculate the volume fraction and then estimate the thickness of each adsorbed polyelectrolyte layer.

Therefore, IRS did not only enable real-time monitoring of the multilayer formation but also, in combination with Maxwell-Garnett theory, allowed us to estimate the thickness of each polyelectrolyte layer (Table S1, Supporting Information). In this calculation, the assumption was made that the layers were homogeneously deposited over the entire length of pAAO pore wall.

Table S1, Supporting Information, shows that the thickness decreases along with increasing number of cycles. This can be attributed to both steric effects causing diffusion problems throughout the porous layer with decreasing orifice diameter with successive LbL deposition cycles.[20] From Table S1, Supporting Information, it can also be observed that, at the same ionic strength, PLL formed a thicker layer compared to PSS. This is related to the molecular weight, density, and structure of the PLL. At a constant salt concentration, a higher molecular weight polyelectrolyte forms a thicker layer,[40] and in this case, the PLL has a higher molecular weight than the PSS. In addition, PLL is a weak polyelectrolyte, which has a simple linear chain[36,45] and low charge density, making the molecules relatively easy to interact with and adsorb to the surface to form a thicker layer.[36] All these factors support our design to prepare a multilayer PSS–PLL with a thicker PLL layer, which is very useful for our application since PLL is subject to degradation by proteinase K. From the result in Table S1, Supporting Information, the total thickness after four deposition cycles is 24.2 nm. This is close to the average pore diameter of 30 nm multilayer thickness already blocking the pAAO pores with a pore diameter of 30 nm (Figure S1c, Supporting Information), which does not take the APTES coating into consideration yet.

Effect of pAAO Layer Thickness on LbL Deposition. In order to examine whether changes in pAAO thickness (at constant pore size) affect the LbL process, we prepared three different pAAO samples ranging in thickness from 1.3 to 3.0 μm and finally 4.4 μm (Figure S1d–f, Supporting Information). Multilayers of PSS and PLL were built up in each pAAO sample from polyelectrolyte solutions of identical concentration. The corresponding EOT changes for successive layers of PSS and PLL and for successive LbL cycles are presented in Figure 2.

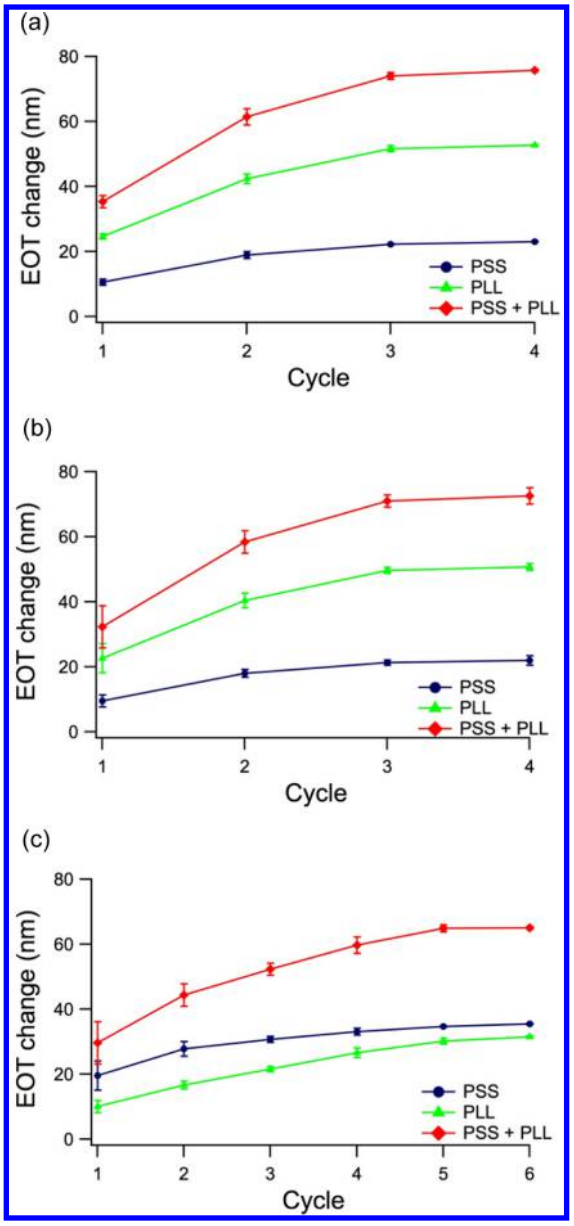

Figure 2. EOT shifts for successive PSS and PLL layers deposited in the pAAO film anodized for (a) 10 min, (b) 20 min, and (c) 30 min producing thicknesses of 1.3, 3.0, and 4.4 μm, respectively. The error bars were calculated as standard deviation from three different experiments.

For the 1.3 to 3.0 μm thick pAAO samples, the results were similar and after four LbL cycles the EOT reached a plateau, indicating pore filling or blocking. For both thicknesses, the PLL incubation gave rise to an EOT shift (53 and 51 nm for a 1.3 and 3.0 μm thickness, respectively) more than double compared to the PSS (23 and 22 nm for 1.3 and 3 μm, respectively). This result confirms that the PLL layer was thicker than the PSS layer. The total EOT change for four LbL cycles was about 76 and 74 nm corresponding to a 24.2 and 23.3 nm LbL layer thickness, if calculated using the Maxwell-Garnett equation for pAAO with a 1.3 and 3.0 μm layer thickness, respectively.

DOI: 10.1021/ac504626m
Anal. Chem. XXXX, XXX, XXX–XXX

The results of LbL deposition in the 4.4 μm thick pAAO sample are shown in Figure 2c. It is clear that this sample showed a rather different trend from the thinner pAAO films. First, the EOT only leveled off after six LbL cycles deposited in the pAAO. This suggests that there were diffusion limitations in the thicker porous layer that resulted in formation and incomplete layers, which were built up in subsequent cycles. Interestingly, the total EOT shift of 65 nm was slightly lower than for the thinner samples after four cycles, suggesting that even after six cycles there were still sites that were not filled in the pores. Second, in contrast to the other two samples, the EOT shift in response to incubation with PSS exceeded that for PLL. This anomaly may be due to the difficulty of PLL to diffuse into a deeper porous layer.

Proteinase K Detection. The LbL coated pAAO film was then utilized as a sensing platform to detect proteinase K, which cleaves peptide bonds of the PLL, including those between lysine amino acids. The PLL layer therefore acted as biorecognition element in our biosensor. We hypothesized that the digestion of the PLL in the pores would destabilize the LbL coating[30,31] and that part of the coating either would be solubilized and diffuse out or could be rinsed out in a subsequent step. Either effect would lead to a blue shift in the EOT.

Our experimental design gave consideration to the influence of porous layer thickness in the interaction between the LbL and the enzyme. The experiments were therefore done for LbL-coated pAAO samples with different film thicknesses. Samples were placed in a flow cell, and solution was pumped across with a flow rate of 0.2 mL/min while monitoring the EOT of the pAAO using IRS. In the first 10 min, the sample was exposed to water, followed by 0.5 mg/mL proteinase K in buffer for 30 min and rinsing with water for 50 min. Representative sensorgrams for the three samples are shown in Figure 3.

The sensorgrams for pAAO samples of 1.3 μm (Figure 3a) and 3.0 μm (Figure 3b) thicknesses presented a similar trend: upon exposure of the 1.3 μm thick surface to the enzyme, the EOT decreased by about 1.9 nm, and then after washing the surface, the EOT blue-shifted by a further 5.2 nm. The first decrease in EOT was due to the digestion of peptide bonds of PLL by the enzyme and diffusion of soluble fragments out of the porous layer. The EOT decrease during the washing step was assumed to be a result of rinsing out of the larger LbL fragments.

For the same concentration of proteinase K, in the functionalized pAAO with a thickness of 3.0 μm (Figure 2b), the EOT blue-shifted by about 1.8 nm when the surface was exposed to the enzyme and about 1.9 nm after rinsing. Therefore, the total decrease in EOT during sensing was 7.1 and 3.7 nm for pAAO with the thickness of 1.3 and 3.0 μm, respectively.

Interestingly, the 4.4 μm sample showed a very different result (Figure 2c). Exposing the proteinase K to the pAAO red-shifted EOT. This suggests that the thick sample diffusion of the PLL fragments was hindered, perhaps due to the higher sample thickness, and that enzyme was incorporated into the porous layer, increasing the net refractive index.

The results show that the thickness of the pAAO is a determinant of the sensor performance possibly due to the fact that diffusion of enzyme in and of polyelectrolyte fragment out of the porous layer is influenced by the layer thickness. Therefore, we decided to use the 1.3 μm thick LbL coated pAAO for the next section.

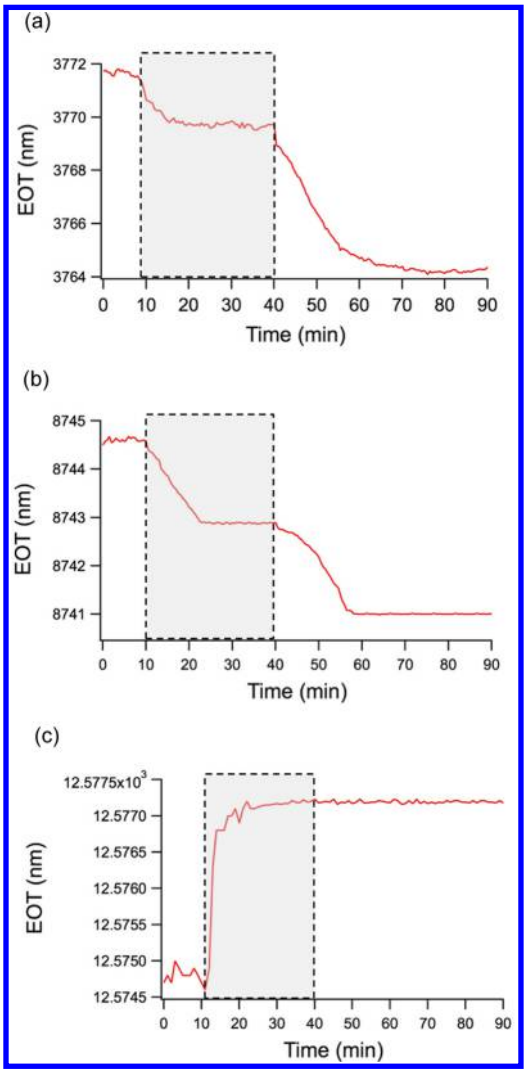

Figure 3. IRS sensorgram during incubation with proteinase K for a 4-cycle of LbL coated pAAO with thickness of 1.3 μm (a) and 3 μm (b) and a 6-cycle of LbL coated pAAO with a thickness of 4.4 μm (c). The gray zone indicates the period of 0.5 mg/mL of proteinase K incubation. Milli-Q water was flown through the surface before and after proteinase K incubation (outside gray area).

SEM was used to investigate the difference between thin and thick pAAO samples further, before degradation (after LbL deposition) and after degradation. The top-view SEM image of functionalized pAAO with the thickness of 1.3 μm shows that the pores were completely blocked after four deposition cycles (Figure S3a, Supporting Information) and opened after enzyme degradation (Figure S3b, Supporting Information). These results were in agreement with the optical detection by IRS showing the decrease in EOT during proteinase K exposure. While in the functionalized pAAO with a thickness of 4.4 μm, the SEM images show that the pores were closed after six deposition cycles (Figure S3c, Supporting Information). However, after incubation with proteinase K, some of the pores were opened while others remained closed (Figure S3d, Supporting Information).

Biosensing Performance. We next determined the biosensing performance in terms of response time and sensitivity. When exposing the LbL coated pAAO to the same concentration of proteinase K (0.5 mg/mL) for different incubation times, the EOT blue shifts increased from 0.9 to 3.0

DOI: 10.1021/ac504626m
Anal. Chem. XXXX, XXX, XXX−XXX

and 6.1 nm, for 7.5, 15, and 30 min incubation times, respectively (Figure 4a). The result in Figure 4a confirmed that,

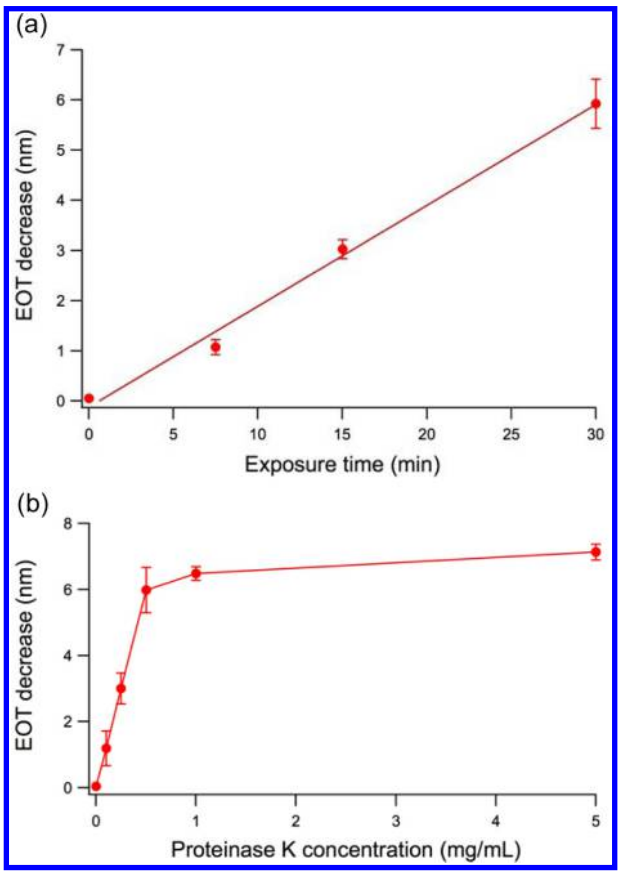

Figure 4. (a) The decrease in EOT observed on LbL coated pAAO for different incubation times (0, 7.5, 15, and 30 min) with proteinase K with the red trace indicates a linear fit. (b) The decrease in EOT observed when the LbL coated pAAO surface was exposed for 30 min to different concentrations of proteinase K. The error bars were calculated as standard deviation from three separated experiments.

the longer the exposure time, the higher is the response change in EOT, since more peptide bonds were cleaved. Incubation times below 10 min were sufficient to obtain a biosensor response.

When increasing concentrations of proteinase K were exposed to the LbL coated pAAO for 30 min, the EOT blue shifts were linear with increasing proteinase K concentration from 0 to 0.5 mg/mL with the linear regression equation of $y = 12.311x - 0.0069$ ($R^2 = 0.99955$) (Figure 4b). Further increases in proteinase K concentration produced further blue shifts but appeared to reach a plateau, presumably because most of the PLL was already digested at a lower enzyme concentration. The lowest proteinase K concentration detected was 0.1 mg/mL. However, the limit of detection (LOD) was calculated using the equation of $LOD = \gamma_b + 3Std_b$, where γ_b is the concentration of blank (concentration in the absence of proteinase K) and Std_b is the standard deviation of blank measurement. Using this equation, the calculated LOD was 0.06 mg/mL.

Enzyme Detection in Chronic Wound Fluid. Finally, the pAAO biosensing platform was utilized to detect the proteinase K enzyme in human wound fluid since *Pseudomonas aeruginosa*, which produces proteinases, is found in chronic wounds and has a propensity to form biofilms.[23,24] The sensorgram collected from the IRS can be seen in Figure 5. Shortly after

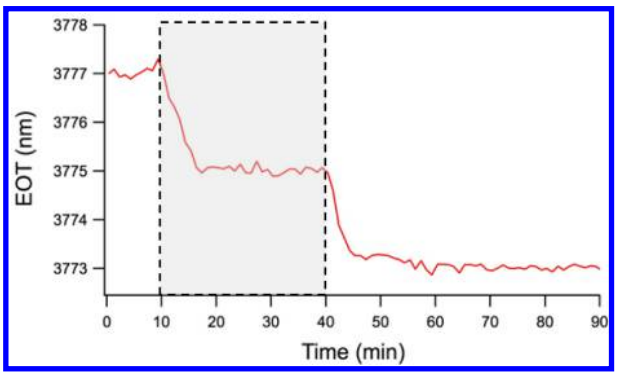

Figure 5. Sensorgram during wound fluid experiment. The LbL coated pAAO sample was exposed to water (0−10 min), a 10-fold dilution of chronic wound fluid spike with 0.5 mg/mL proteinase K (11−40 min, denoted by the gray box) and water (41−90 min).

wound fluid spiked with 0.5 mg/mL proteinase K was introduced to the LbL coated pAAO sample, the EOT decreased gradually for 8 min (from 11 to 18 min) and reached a constant value after 19 min of wound fluid exposure. The decrease in EOT (about 2.1 nm) confirms the presence of proteinase K in the wound fluid sample degrading the peptide bonds of PLL deposited in the pAAO. The washing step led to a further blue shift by about 2.1 nm, bringing the total decrease in EOT during wound fluid sensing to about 4.2 nm. If this value is plotted into the linear equation obtained from the EOT shift versus the concentration curve in Figure 4b, a proteinase K concentration of 0.34 ± 0.18 mg/mL is obtained. This concentration value is in close proximity with the proteinase K concentration spiked in the wound fluid indicating a small matrix interference effect. In the real wound fluid sample, as mentioned in the introduction, the determination of bacterial infection is conducted in culture media. To the best of our knowledge, there is no report in regards to a quantitative analysis of proteinases in the wound fluid sample. One paper from Woods et al. reports the *Pseudomonas aeruginosa* strain in some clinical samples, and they found 0.104 ± 0.037 mg/mL protease produced by *Pseudomonas aeruginosa* in the burn injury sample.[46] This value is reasonably close to the concentration of proteinase K spiked in the wound fluid sample used in this experiment.

CONCLUSIONS

We have fabricated a label-free pAAO-based interferometric biosensing platform using LbL deposition with PSS and PLL polyelectrolytes. The peptide bonds of PLL acted as a biorecognition component of the biosensor since the proteinase K could easily cleave this component. LbL coating and degradation of the PLL layer by proteinase K were monitored in real time using IRS. Red shifts in EOT during LbL deposition confirmed the layer formation, while decreases in EOT were observed upon incubation with proteinase K, hence transducing the digestion of the PLL layer into optical effects. Finally, we demonstrated the application of this biosensor to the detection of bacterial enzyme spiked in a human wound fluid sample. This biosensing platform appears to be suitable for further development into a point-of-care diagnostic of pathogenic bacterial infections in chronic wounds.

DOI: 10.1021/ac504626m
Anal. Chem. XXXX, XXX, XXX−XXX

■ ASSOCIATED CONTENT

Supporting Information

Figure S1, the SEM images of pAAO anodized at a constant voltage of 40 V. Table S1, the thickness of the PSS and PLL layer calculated by the Maxwell-Garnett equation. Figure S2, the top-view SEM images of pAAO beforethe deposition cycles, after two deposition cycles, and after four deposition cycles. Figure S3, the SEM images of LbL coated pAAO before and after incubation with proteinase K. This material is available free of charge via the Internet at http://pubs.acs.org/.

■ AUTHOR INFORMATION

Corresponding Authors

*E-mail: nico.voelcker@unisa.edu.au.
*E-mail: schoenherr@chemie.uni-siegen.de.

Author Contributions

The manuscript was written through contributions of all authors. All authors have given approval to the final version of the manuscript.

Notes

The authors declare no competing financial interest.

■ ACKNOWLEDGMENTS

The authors would like to thank Allison Cowin and Elizabeth Melville for providing human wound fluid samples, Marc Steuber for FE-SEM analyses, Imad Zamrik for assistance in calculating of layer thickness, Katrin-Stephanie Tücking for fruitful discussions, Dipl.-Ing. Gregor Schulte for excellent technical support, and Prof. X. Jiang for access to the FE-SEM. The authors would like to acknowledge the support of the Australian Government's Cooperative Research Centres Program. The authors also gratefully acknowledge financial support from the EU (FP7 project BacterioSafe, Grant no. 245500, FP7Marie Curie Actions, project KOALA, Grant no. 295155), the DAAD for a PhD scholarship for H.B., the ATN-DAAD grant scheme for providing travel funding, in particular funding by the DAAD with financial support of the Bundesministerium für Bildung und Forschung BMBF, Wound Management Innovation CRC, and the University of South Australia for a top-up and PhD scholarship for F.S.H.K.

■ REFERENCES

(1) Dronov, R.; Jane, A.; Shapter, J. G.; Hodges, A.; Voelcker, N. H. *Nanoscale* **2011**, *3*, 3109−3114.
(2) Jani, A. M. M.; Losic, D.; Voelcker, N. H. *Prog. Mater. Sci.* **2013**, *58* (5), 636−704.
(3) Kumeria, T.; Santos, A.; Losic, D. *Sensors* **2014**, *14*, 11878−11918.
(4) Santos, A.; Kumeria, T.; Losic, D. *Trends Anal. Chem.* **2013**, *44*, 25−38.
(5) Alvarez, S. D.; Li, C.-P.; Chiang, C. E.; Schuller, I. K.; Sailor, M. J. *ACS Nano* **2009**, *3* (10), 3301−3307.
(6) Santos, A.; Balderrama, V. S.; Alba, M.; Formentin, P.; Ferre-Borrull, J.; Pallares, J.; Marsal, L. F. *Nanoscale Res. Lett.* **2012**, *7* (1), 370−373.
(7) Santos, A.; Balderrama, V. S.; Alba, M.; Formentin, P.; Ferre-Borrull, J.; Pallares, J.; Marsal, L. F. *Adv. Mater.* **2012**, *24*, 1050−1054.
(8) Santos, A.; Kumeria, T.; Losic, D. *Trends Anal. Chem.* **2013**, *44*, 25−38.
(9) Santos, A.; Kumeria, T.; Losic, D. *Anal. Chem.* **2013**, *85*, 7904−7911.
(10) Santos, A.; Macias, G.; Ferre-Borrull, J.; Pallares, J.; Marsal, L. F. *Appl. Mater. Interfaces* **2012**, *4*, 3584−3588.
(11) Krismastuti, F. S. H.; Brooks, W. L. A.; Sweetman, M. J.; Sumerlin, B. S.; Voelcker, N. H. *J. Mater. Chem. B* **2014**, *2* (25), 3972−3983.
(12) Krismastuti, F. S. H.; Cowin, A. J.; Pace, S.; Melville, E.; Dargaville, T. R.; Voelcker, N. H. *Aust. J. Chem.* **2013**, *66* (11), 1428−1434.
(13) Pace, S.; Vasani, R. B.; Cunin, F.; Voelcker, N. H. *New J. Chem.* **2013**, *37*, 228−235.
(14) Jani, A. M. M.; Anglin, E. J.; McInnes, S. J. P.; Losic, D.; Shapter, J. G.; Voelcker, N. H. *Chem. Commun.* **2009**, 3062−3064.
(15) Jani, A. M. M.; Kempson, I. M.; Losic, D.; Voelcker, N. H. *Angew. Chem.* **2010**, *122*, 8105−8109.
(16) Sun, L.; Dai, J.; Baker, G. L.; Bruening, M. L. *Chem. Mater.* **2006**, *18*, 4033−4039.
(17) Yamaguchi, A.; Uejo, F.; Yoda, T.; Uchida, T.; Tanamura, Y.; Yamashita, T.; Teramae, N. *Nat. Mater.* **2004**, *3*, 337−341.
(18) Carrillo, J.-M. Y.; Dobrynin, A. V. *ACS Nano* **2011**, *5* (4), 3010−3019.
(19) Lazzara, T. D.; Lau, K. H. A.; Abou-Kandil, A. I.; Caminade, A.-M.; Majoral, J.-P.; Knoll, W. *ACS Nano* **2010**, *4* (7), 3909−3920.
(20) Lazzara, T. D.; Lau, K. H. A.; Knoll, W.; Janshoff, A.; Steinem, C. *Beilstein J. Nanotechnol.* **2012**, *3*, 475−484.
(21) Johansson, A.; Lu, J.; Carlsson, J.-O.; Boman, M. *J. Appl. Phys.* **2004**, *96* (9), 5189−5194.
(22) Dargaville, T. R.; Farrugia, B. L.; Broadbent, J. A.; Pace, S.; Upton, Z.; Voelcker, N. H. *Biosens. Bioelectron.* **2013**, *41*, 30−42.
(23) Kirketerp-Møller, K.; Jensen, P. Ø.; Fazli, M.; Madsen, K. G.; Pedersen, J.; Moser, C.; Tolker-Nielsen, T.; Hoiby, N. H.; Givskov, M.; Bjarnsholt, T. *J. Clin. Microbiol.* **2008**, *46* (8), 2717−2722.
(24) Nakagami, G.; Sanada, H.; Sugama, J.; Morohoshi, T.; Ikeda, T.; Ohta, Y. *Wound Rep. Reg.* **2008**, *16*, 30−36.
(25) Bjarnsholt, T.; Kirketerp-Møller, K.; Jensen, P. Ø.; Madsen, K. G.; Phipps, R.; Krogfelt, K.; Hoiby, N. H.; Givskov, M. *Wound Rep. Reg.* **2008**, *16* (1), 2−10.
(26) Bjarnsholt, T.; Kirketerp-Møller, K.; Kristiansen, S.; Phipps, R.; Nielsen, A. K.; Jensen, P. Ø.; Høiby, N.; Givskov, M. *APMIS* **2007**, *115*, 921−928.
(27) Goldschmidt, P.; Degorge, S.; Merabet, L.; Chaumeil, C. *PLoS One* **2014**, *9* (6), No. e94886.
(28) Tücking, K.-S.; Handschuh-Wang, S.; Schönherr, H. *Aust. J. Chem.* **2014**, *67* (4), 578−584.
(29) Morihara, K. *J. Bacteriol.* **1964**, *88* (3), 745−757.
(30) Kilian, K. A.; Lai, L. M. H.; Magenau, A.; Cartland, S.; Bocking, T.; Girolamo, N. D.; Gal, M.; Gaus, K.; Gooding, J. J. *Nano Lett.* **2009**, *9* (5), 2021−2025.
(31) Orosco, M. M.; Pacholski, C.; Miskelly, G. M.; Sailor, M. J. *Adv. Mater.* **2006**, *18*, 1393−1396.
(32) Raoufi, M.; Schönherr, H. *RSC Adv.* **2013**, *3*, 13429−13436.
(33) Raoufi, M.; Tranchida, D.; Schönherr, H. *Langmuir* **2012**, *28* (26), 10091−10096.
(34) Masuda, H. Highly Ordered Nanohole Arrays in Anodic Porous Alumina. In *Ordered Porous Nanostructures and Applications*; Wehrspohn, R. B., Ed.; Springer: New York, 2005; pp 37−55.
(35) Masuda, H.; Fukuda, K. *Science* **1995**, *268* (5216), 1466−1468.
(36) Burke, S. E.; Barret, C. J. *Biomacromolecules* **2003**, *4*, 1773−1783.
(37) Fery, A.; Schöler, B.; Cassagneau, T.; Caruso, F. *Langmuir* **2001**, *17* (13), 3779−3783.
(38) Mendelsohn, J. D.; Barret, C. J.; Chan, V. V.; Pal, A. J.; Mayes, A. M.; Rubner, M. F. *Langmuir* **2000**, *16*, 5017−5023.
(39) Roy, C. J.; Dupont-Gillain, C.; Demoustier-Champagne, S.; Jonas, A. M.; Landoulsi, J. *Langmuir* **2010**, *26* (5), 3350−3355.
(40) Seyrek, E.; Hierrezuelo, J.; Sadeghpour, A.; Szilagyi, I.; Borkovec, M. *Phys. Chem. Chem. Phys.* **2011**, *13*, 12716−12719.
(41) Burke, S. E.; Barrett, C. J. *Pure Appl. Chem.* **2004**, *76* (7−8), 1387−1398.
(42) Decher, G.; Schmitt, J. *Prog. Colloid Polym. Sci.* **1992**, *89*, 160−164.
(43) Aspnes, D. E. *Thin Solid Films* **1982**, *89*, 249−262.

DOI: 10.1021/ac504626m
Anal. Chem. XXXX, XXX, XXX−XXX

(44) Aspnes, D. E. *Am. J. Phys.* **1981**, *50* (8), 704−709.
(45) Yasui, S. C.; Keiderling, T. A. *J. Am. Chem. Soc.* **1986**, *108* (18), 5576−5581.
(46) Woods, D. E.; Schaffer, M. S.; Rabin, H. R.; Campbell, G. D.; Sokol, P. A. *J. Clin. Microbiol.* **1986**, *24* (2), 260−264.

DOI: 10.1021/ac504626m
Anal. Chem. XXXX, XXX, XXX−XXX